Int. J. Heat Mass Transfer. Vol. 30, No. 2, pp. 263–273, 1987
Printed in Great Britain

0017–9310/87 $3.00+0.00
Pergamon Journals Ltd.

Thermal convection associated with hot/cold pipes buried in a semi-infinite, saturated, porous medium

K. HIMASEKHAR† and HAIM H. BAU

Department of Mechanical Engineering and Applied Mechanics, University of Pennsylvania, 111 Towne Building/D3, Philadelphia, PA 19104-6315, U.S.A.

(*Received* 20 *December* 1985 *and in final form* 28 *May* 1986)

Abstract—Analytical and numerical solutions are presented for steady-state, thermal convection induced by hot/cold pipes buried in a saturated, semi-infinite, permeable medium, the surface of which is horizontal, impermeable and subject to Robin's (convective) boundary condition. The pipe's surface is impermeable and isothermal. The analytical solution consists of the construction of a double expansion in terms of the Rayleigh and the inverse Biot numbers. Computer algebra (MACSYMA) is used to carry out the more tedious mathematical manipulations. The numerical approach involves both the construction of a regular perturbation expansion in terms of the Rayleigh number and the solution of the full nonlinear governing equations. The results of the perturbative analysis and the numerical calculations, which include descriptions of the flow and temperature fields as well as correlations for the Nusselt number, are compared and found to agree favorably.

1. INTRODUCTION

THE PROBLEM of heat losses from buried pipes has received considerable attention in recent years. This problem arises, for example, in connection with underground electrical power transmission lines, burial of nuclear waste, and oil/gas pipe lines in which the oil/gas is heated or chilled in order to reduce the pumping costs.

Most of the existing heat transfer calculations only take into account conduction [1–4]. However, in many cases, the medium is permeable to fluid motion, and the temperature difference between the pipe and the medium surface may cause thermal convection. Indeed, where the medium is permeable, the role played in the heat transfer process by the free convective effects typically is as important as that played by the conductive effects.

In spite of this fact, very little has been done to study the thermal convection associated with pipes buried in a permeable medium. To date, Schrock *et al.* [5], Fernandez and Schrock [6] and Farouk and Shayer [7] have carried out numerical analyses and experiments for a hot cylinder buried beneath a permeable horizontal surface; and Bau [8] has obtained a low Rayleigh number analytical solution for pipes buried beneath both permeable and impermeable, isothermal surfaces. Unfortunately, the utility of the analytical solution presented in the latter work is limited in that the isothermal surface is an idealization. In practice, one would expect to observe temperature variations along the medium's surface.

In the present work, we extend the work presented in ref. [8] to include Robin's (convective) boundary condition at the medium's surface. We use a variety of analytical and numerical tools to obtain descriptions of the flow and temperature fields around the buried pipe as well as correlations for the heat transfer. In Section 2 we formulate the mathematical problem. In Section 3 we solve the governing equations using regular perturbation expansions. The perturbation expansion is instrumental in the construction of a correlation for the Nusselt number. The nonlinear governing equations are also solved numerically (Section 4). The numerical solution is used to verify and establish the range of utility of the heat transfer correlation developed in Section 3. The results of the perturbative analysis and the numerical simulation are described and discussed in Section 5.

2. MATHEMATICAL MODEL

Consider a pipe of radius $\hat{r}_1$ buried at a depth of $\hat{d}$ beneath the horizontal, impermeable, surface of a semi-infinite, fully saturated porous medium (Fig. 1). The pipe's surface is maintained at a uniform temperature $\hat{T}_1$ such as might be the case when there is turbulent flow inside the pipe. The ambient above the semi-infinite medium is maintained at constant temperature $\hat{T}_2$. As a result of the temperature difference between the pipe's surface and the ambient, $(\hat{T}_1 - \hat{T}_2)$, motion is induced in the medium. The symbol $\hat{}$ in the above expression denotes the dimensional form of variables which will later be made nondimensional. Robin's (convective) boundary condition is imposed on the medium's surface.

It is convenient to formulate this problem using bicylindrical coordinates [10] since the boundaries can be prescribed along constant coordinate lines.

† On study leave from the Department of Mechanical Engineering, Andhra University, Waltair, 530003 India.

NOMENCLATURE

a	scale factor for the bicylindrical coordinates ($\sinh \alpha_1$)
Bi	Biot number, $h\hat{r}_1/k_{eq}$
Bi_{eff}	effective Biot number, $Bi\hat{d}/\hat{r}_1$
d_p	characteristic dimension of the porous medium
d	burial depth, $\hat{d}/\hat{r}_1$
$g(\alpha, \beta)$	a metric coefficient, equation (5)
g^*	gravitational acceleration
G, H	functions, equation (5)
h	convective heat transfer coefficient at the medium's surface
k_{eq}	equivalent thermal conductivity of the porous medium
N_s	coefficients in the expansion for the Nusselt number, equation (6)
Nu	Nusselt number, Q/Q_{cond}
Pr	Prandtl number, ν/α_{eq}
Q	heat flow per unit length of the pipe, $\hat{Q}/k_{eq}(\hat{T}_1 - \hat{T}_2)$
q	heat flux on the pipe's surface or on the medium's surface, $\hat{q}\hat{r}_1/k_{eq}(\hat{T}_1 - \hat{T}_2)$
Ra	Darcy–Rayleigh number, $g^*\beta(\hat{T}_1 - \hat{T}_2)\lambda\hat{r}_1/\nu\alpha_{eq}$
Ra_{eff}	effective Darcy–Rayleigh number, $Ra\hat{d}/\hat{r}_1$
Re	Reynolds number
$\hat{r}_1$	radius of the pipe
T	temperature, $(\hat{T} - \hat{T}_2)/(\hat{T}_1 - \hat{T}_2)$
X, Y	Cartesian coordinates (Fig. 1).

Greek symbols

α, β	bicylindrical coordinates defined by equation (1)
α_{eq}	equivalent thermal diffusivity of the porous medium
β^*	thermal expansion coefficient of the saturating fluid
λ	permeability
ν	kinematic viscosity of the saturating fluid
ψ	streamfunction.

Subscripts

1	pipe surface
2	surface of the semi-infinite medium.

Superscript

$\hat{}$	dimensional quantities.

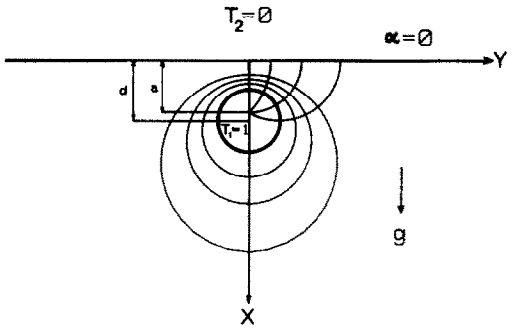

FIG. 1. The geometrical configuration and the coordinate system.

Another advantage of the bicylindrical coordinate system is that it permits us to map the semi-infinite physical domain into a finite rectangle. Thus, when one attempts to solve the problem numerically, one need not truncate the physical domain and impose somewhat arbitrary boundary conditions at the truncation lines as was done in [7].

The conversion of Cartesian coordinates (X, Y) into bicylindrical coordinates (α, β) (Fig. 1) is achieved through the transformation:

$$X + iY = a \coth\left(\frac{\alpha - i\beta}{2}\right) \tag{1}$$

where constant α lines are the circles:

$$(X - a\coth\alpha)^2 + Y^2 = \left(\frac{a^2}{\sinh^2\alpha}\right). \tag{2}$$

The pipe and the medium surface correspond, respectively, to $\alpha = \alpha_1$ and $\alpha = 0$. The scaling factor can be expressed as $a = \sinh\alpha_1$ and the burial depth as $d = \cosh\alpha_1$.

The fluid motion is described by two-dimensional Darcy–Oberbeck–Boussinesq equations:

$$\frac{\partial^2\psi}{\partial\alpha^2} + \frac{\partial^2\psi}{\partial\beta^2} = aRa\left[G(\alpha,\beta)\cdot\frac{\partial T}{\partial\alpha} + H(\alpha,\beta)\cdot\frac{\partial T}{\partial\beta}\right]$$
$$\frac{\partial^2 T}{\partial\alpha^2} + \frac{\partial^2 T}{\partial\beta^2} = \frac{\partial\psi}{\partial\alpha}\cdot\frac{\partial T}{\partial\beta} - \frac{\partial\psi}{\partial\beta}\cdot\frac{\partial T}{\partial\alpha} \tag{3}$$

with the boundary conditions

$$\psi = 0 \quad T = 1 \quad \text{at } \alpha = \alpha_1$$

$$\psi = 0 \quad \frac{\partial T}{\partial\alpha} = Big^{1/2}(\alpha,\beta)\cdot T \quad \text{at } \alpha = 0$$

and the symmetry conditions

$$\psi = \frac{\partial T}{\partial\beta} = 0 \quad \text{at } \beta = 0, \pi. \tag{4}$$

In the above

$$H(\alpha,\beta) = \frac{1 - \cosh\alpha\cdot\cos\beta}{(\cosh\alpha - \cos\beta)^2}$$

$$G(\alpha,\beta) = \frac{\sinh\alpha\cdot\sin\beta}{(\cosh\alpha - \cos\beta)^2} \tag{5}$$

and

$$g(\alpha,\beta)=\left(\frac{a}{\cosh\alpha-\cos\beta}\right)^2.$$

Equations (3)–(5) are written in nondimensional form. The length scale is the pipe's radius, $\hat{r}_1$; the velocity scale is $\alpha_{eq}/\hat{r}_1$; and the temperature scale is $(\hat{T}_1-\hat{T}_2)$. The Darcy–Rayleigh number (Ra) and the Biot number (Bi) are based on the pipe's radius. Hence

$$Ra=\frac{g^*\beta^*\lambda\hat{r}_1(\hat{T}_1-\hat{T}_2)}{\alpha_{eq}\nu}\quad\text{and}\quad Bi=\frac{h\hat{r}_1}{k_{eq}}. \tag{6}$$

The effective Rayleigh and Biot numbers differ from the above and are proportional to the burial depth, so that

$$Ra_{eff}=Ra\cosh\alpha_1\quad\text{and}\quad Bi_{eff}=Bi\cosh\alpha_1.$$

Note that $Ra>0$ corresponds to a hot pipe buried beneath a cold surface ($\hat{T}_1>\hat{T}_2$) or a cold pipe ($\hat{T}_1<\hat{T}_2$) installed above a hot surface. On the other hand, $Ra<0$ corresponds to a cold pipe ($\hat{T}_1<\hat{T}_2$) buried beneath a hot surface or a hot pipe located above a cold surface. In the latter two cases, one should invert the direction of the gravity vector in Fig. 1.

The local heat flux (q) at the pipe's surface ($\alpha=\alpha_1$) or at the medium's surface ($\alpha=0$) can be calculated in terms of temperature as:

$$q=\left(\frac{\cosh\alpha-\cos\beta}{a}\right)\cdot\left.\frac{\partial T}{\partial\alpha}\right|_{\alpha=0\text{ or }\alpha_1}. \tag{7}$$

The heat flow (Q) per unit length of the pipe is

$$Q=\int_{-\pi}^{\pi}\left.\left(\frac{\partial T}{\partial\alpha}\right)\right|_{\alpha=0\text{ or }\alpha_1}\mathrm{d}\beta. \tag{8}$$

The Nusselt number (Nu) is defined as the ratio of the total heat flow (Q) and the heat flow in the absence of convection (Q_{cond})

$$Nu=Q/Q_{cond}. \tag{9}$$

Unfortunately, no exact expression for Q_{cond} is available; so we rely on the following approximate expression for Q_{cond} which was reported in [4]

$$Q_{cond}\approx aBi[(1+aBi\alpha_1)^2-1]^{-1/2}. \tag{10}$$

According to ref. [4] and to subsequent calculations carried out here, this expression is accurate within 4% for $(aBi)\geqslant 1$.

3. SMALL RAYLEIGH NUMBER SOLUTION—A PERTURBATION EXPANSION

No exact solution is known for equations (3)–(5). In this section, we describe a perturbative analysis which allows us to obtain approximate solutions for small values of the Rayleigh number. To this end, we consider the dependent variables (ψ, T) to be functions of both the coordinates (α, β) and the Rayleigh number (Ra). Next, we expand the dependent variables into Taylor series in terms of Ra:

$$T(\alpha,\beta;Ra)=\sum_{s=0}^{\infty}Ra^sT_s(\alpha,\beta),$$

$$\psi(\alpha,\beta;Ra)=\sum_{s=1}^{\infty}Ra^s\psi_s(\alpha,\beta) \tag{11}$$

$$Q(Ra)=\sum_{s=0}^{\infty}Ra^sQ_s\quad\text{and}\quad Nu(Ra)=\sum_{s=0}^{\infty}Ra^sN_s$$

where the terms with index s are the coefficients in the Taylor expansions.

By introducing these expansions (11) into the differential equations (3)–(5) and comparing coefficients of like powers in s, we obtain an infinite set of linear partial differential equations

$$\frac{\partial^2T_0}{\partial\alpha^2}+\frac{\partial^2T_0}{\partial\beta^2}=0,\quad\psi_0=0$$

$$\frac{\partial^2\psi_s}{\partial\alpha^2}+\frac{\partial^2\psi_s}{\partial\beta^2}=G(\alpha,\beta)\frac{\partial T_{s-1}}{\partial\alpha}+H(\alpha,\beta)\frac{\partial T_{s-1}}{\partial\beta} \tag{12}$$

and

$$\frac{\partial^2T_s}{\partial\alpha^2}+\frac{\partial^2T_s}{\partial\beta^2}=\sum_{j=1}^{s}\frac{\partial(\psi_j,T_{s-j})}{\partial(\alpha,\beta)}\quad(s\geqslant 1)$$

with the boundary conditions:

$$T_0=1,\quad T_s=0,\quad\psi_s=0\quad(s\geqslant 1)\quad\text{at }\alpha=\alpha_1$$

$$\frac{\partial T_s}{\partial\alpha}=Big^{1/2}(\alpha,\beta)T_s,\quad\psi_s=0\quad(s\geqslant 0)\quad\text{at }\alpha=0$$

$$\frac{\partial T_s}{\partial\beta}=\psi_s=0\quad\text{at }\beta=0,\pi.$$

At each level of approximation, the respective contributions to the heat flow and to the Nusselt number are:

$$Q_s=\int_{-\pi}^{\pi}\left(\frac{\partial T_s}{\partial\alpha}\right)_{\alpha=0\text{ or }\alpha_1}\mathrm{d}\beta\quad\text{and}\quad N_s=\frac{Q_s}{Q_{cond}}.$$

In an earlier paper [8], one of us obtained analytical solutions for equations (12), for $s\leqslant 3$, for the special case of an isothermal top boundary ($Bi\to\infty$). Unfortunately, for the more general case of finite Bi, a closed-form analytical solution is not feasible because of the appearance of the metric coefficient $g^{1/2}(\alpha,\beta)$, in Robin's boundary condition at $\alpha=0$ [3, 4]. In this paper, we use two different approaches to overcome this difficulty, one analytical and one numerical. Per the numerical approach described in Section 3.2, we solve the equations in (12) using finite differences. Per the analytical approach described in Section 3.1, we further expand the dependent variables into Taylor series in terms of the inverse of the Biot number (Bi^{-1}).

The rationale for the deployment of the analytical tool is two fold. First, the numerical solution predicts extremely small corrections at $O(Ra)$ which may be subject to numerical error. Thus, it is desirable to obtain analytical expressions as well. Second, it gives us the opportunity to demonstrate the usefulness of computer algebra in heat transfer analysis.

3.1. *Analytical solution—a double expansion in Ra and Bi*

In order to solve equations (12) analytically, we further expand the dependent variables (T_s, ψ_s) into Taylor series in terms of Bi^{-1}:

$$T_s = \sum_{p=0}^{\infty} Bi^{-p} T_{s,p}(\alpha,\beta), \quad \psi_s = \sum_{p=0}^{\infty} Bi^{-p}\psi_{s,p}(\alpha,\beta)$$
$$Q_s = \sum_{p=0}^{\infty} Bi^{-p} Q_{s,p} \quad \text{and} \quad N_s = \sum_{p=0}^{\infty} Bi^{-p} N_{s,p}. \tag{13}$$

By introducing the above expansions into the partial differential equations and equating coefficients of like powers of Bi, we obtain the following set of linear partial differential equations:

$$\frac{\partial^2 T_{0,p}}{\partial\alpha^2}+\frac{\partial^2 T_{0,p}}{\partial\beta^2} = 0$$
$$\frac{\partial^2 T_{s,p}}{\partial\alpha^2}+\frac{\partial^2 T_{s,p}}{\partial\beta^2} = \sum_{j=1}^{s}\sum_{k=0}^{p}\frac{\partial(\psi_{j,k}, T_{s-j,p-k})}{\partial(\alpha,\beta)} \tag{14}$$
$$\frac{\partial^2 \psi_{s,p}}{\partial\alpha^2}+\frac{\partial^2 \psi_{s,p}}{\partial\beta^2} = G(\alpha,\beta)\frac{\partial T_{s-1,p}}{\partial\alpha}+H(\alpha,\beta)\frac{\partial T_{s-1,p}}{\partial\beta}$$

with the boundary conditions:

$$\left.\begin{array}{l} T_{0,0} = 1; \quad T_{0,p} = 0 \quad (p \geq 1); \\ T_{s,p} = \psi_{s,p} = 0 \quad (s \geq 1, p \geq 0) \end{array}\right\} \text{at } \alpha = \alpha_1$$
$$T_{s,0} = 0 \quad (s \geq 0); \tag{15}$$
$$\left.\begin{array}{l} T_{s,p} = \dfrac{1}{g^{1/2}(\alpha,\beta)}\dfrac{\partial T_{s,p-1}}{\partial\alpha} \quad (s \geq 0, p \geq 1), \\ \psi_{s,p} = 0 \quad (s \geq 0, p \geq 0) \end{array}\right\} \text{at } \alpha = 0$$

and

$$\frac{\partial T_{s,p}}{\partial\beta} = \psi_{s,p} = 0 \quad (s \geq 0, p \geq 0) \quad \text{at } \beta = 0, \pi.$$

Also

$$Q_{s,p} = \int_{-\pi}^{\pi}\left(\frac{\partial T_{s,p}}{\partial\alpha}\right)_{\alpha=0 \text{ or } \alpha_1} d\beta \quad \text{and} \quad N_{s,p} = \frac{1}{Q_{0,0}}C_{s,p}$$

where

$$C_{s,p} = Q_{s,p} - \frac{1}{Q_{0,0}}\sum_{k=1}^{p} C_{s,p-k}Q_{0,k}.$$

The advantage of equations (14) over (12) is that they can be solved exactly. To this end, we expand the dependent variables ($\psi_{s,p}$, $T_{s,p}$) into their Fourier series in terms of β. That is:

$$T_{s,p} = \sum_{n=0}^{\infty} f_{s,p,n}(\alpha)\cos n\beta$$
$$\psi_{s,p} = \sum_{n=1}^{\infty} g_{s,p,n}(\alpha)\sin n\beta. \tag{16}$$

Upon substitution of (16) into (14), one obtains equations of the general form

$$\frac{d^2 y}{d\alpha^2} - n^2 y = \text{LHS}(\alpha) \tag{17}$$

where y stands either for $f_{s,p,n}$ or $g_{s,p,n}$ and the LHS is a forcing term which increases in length and complexity as the order of the approximation increases. Fortunately, the tedious repetitive labor of solving equations like (17) can be delegated to the computer. To this end, we use MACSYMA. In Fig. 2, we reproduce a short program which describes the solution procedure for $g_{1,1,n}(\alpha)$. Similar procedures were used to solve the other equations involved.

In Fig. 2, lines labeled (c*i*) and (d*i*) represent the

```
(c1) loadprint:false$
(c2) y:y(x)$
(c3) eq1: diff(y,x,2)-n^2*y=2*n*exp(-n*x)/x1;
                        2                              - n x
                       d              2           2 n %e
(d3)                   --- (y(x)) - n  y(x) = -----------
                         2                          x1
                       dx

(c4) assume(n>0)$
(c5) ode2(eq1,y,x);
                                       - n x
                         (2 n x + 1) %e                 n x          - n x
(d5)          y(x) = - ------------------- + %k1 %e    + %k2 %e
                              2 n x1

(c6) linsolve([subst(x1,x,part(d5,2))=0,subst(0,x,part(d5,2))=0],[%k1,%k2]);
                                                    2 n x1
                          1                       %e       - 2 n x1 - 1
(d6)           [%k1 = ------------, %k2 = ------------------------]
                      2 n x1                          2 n x1
                    %e       - 1          2 n x1 %e       - 2 n x1

(c7) yy:part(d5,2)$
(c8) yy:ratsimp(ev(yy,d6))$
(c9) y(x):=''yy;
                                 2 n x1            2 n x
                             x %e       + (1 - %e      ) x1 - x
(d9)              y(x) := - ---------------------------------
                                   2 n x1 + n x       n x
                               x1 %e              - %e     x1

(c10) quit();
```

FIG. 2. An example of a MACSYMA program for the solution of second-order ODE.

user's input and the machine's response, respectively. For brevity's sake, we denote $g_{1,1,n}$ by y and use x instead of α. In line (c2) we declare y to be a function of x. In line (c3) we type in the corresponding differential equation. The machine responds in line (d3) with a somewhat nicer expression which allows us to verify conveniently the correctness of the input. In line (c5) we invoke the routine (ode 2) which is a solver for ODEs of the second order. The solution appears in line (d5) with two constants of integration %$k1$ and %$k2$. In order to calculate these constants of integration, we utilize the boundary conditions and then solve two linear algebraic equations for %$k1$ and %$k2$ by invoking the linear equations solver (linsolve) in line (c6). The expressions for %$k1$ and %$k2$ appear in line (d6). The variable yy appearing in lines (c7)–(c9) is a dummy variable which is used merely for programming convenience. In the final result listed in line (d9), the undetermined coefficients %$k1$ and %$k2$ are replaced with their corresponding values and the resulting expression is simplified.

Manipulations like those described above allow us to obtain solutions for the streamfunction and the temperature fields. A sample of the results is given below:

$$T_{0,0} = \alpha/\alpha_1$$

$$T_{0,1} = \frac{1}{a}\left[\frac{\alpha_1-\alpha}{\alpha_1^2}+\frac{\sinh(\alpha-\alpha_1)\cos\beta}{\alpha_1\sinh\alpha_1}\right]$$

$$T_{0,2} = \frac{1}{a^2}\left[\frac{\alpha-\alpha_1}{\alpha_1^2}\left(\frac{1}{\alpha_1}+\tfrac{1}{2}\coth\alpha_1\right)\right.$$
$$-\frac{1}{\alpha_1}\left(\frac{1}{\alpha_1}+\coth\alpha_1\right)\frac{\sinh(\alpha-\alpha_1)}{\sinh\alpha_1}\cos\beta \quad (18)$$
$$\left.+\frac{1}{2}\frac{\cosh\alpha_1\sinh 2(\alpha-\alpha_1)\cos 2\beta}{\alpha_1\sinh\alpha_1\sinh 2\alpha_1}\right]$$

$$\psi_{1,0} = a\left[-\frac{1}{2}\frac{\alpha}{\alpha_1}\frac{\sin\beta}{\cosh\alpha-\cos\beta}\right.$$
$$\left.+\sum_{n=1}^{\infty}\mathrm{e}^{-n\alpha_1}\frac{\sinh n\alpha}{\sinh n\alpha_1}\sin n\beta\right]$$

$$\psi_{1,1} = \frac{1}{2\alpha_1}\frac{\sin\beta}{\cosh\alpha-\cos\beta}\left[\frac{\alpha}{\alpha_1}-\frac{1}{2}+\frac{\sinh(\alpha_1-2\alpha)}{2\sinh\alpha_1}\right]$$

etc.

In this section, our prime interest is in obtaining correlations for the heat transfer. Keeping this fact in mind, we can save a considerable amount of effort by considering the relationship

$$Q_{s,p} = -\frac{1}{\alpha_1}\int_0^{2\pi}\left(\frac{1}{g^{1/2}(\alpha,\beta)}\frac{\partial T_{s,p-1}}{\partial\alpha}\right)_{\alpha=0}\mathrm{d}\beta$$
$$-\frac{1}{\alpha_1}\sum_{j=1}^{s}\sum_{k=0}^{p}\int_0^{\alpha_1}\int_0^{2\pi}T_{s-j,p-k}\frac{\partial\psi_{j,k}}{\partial\beta}\mathrm{d}\beta\,\mathrm{d}\alpha$$
$$\text{with } s\geqslant 1, p\geqslant 1. \quad (19)$$

The foregoing can be rewritten as

$$Q_{s,p} = -\frac{2\pi}{a\alpha_1}\left[f'_{s,p-1,0}(0)-\tfrac{1}{2}f'_{s,p-1,1}(0)\right]$$
$$-\frac{\pi}{\alpha_1}\sum_{j=1}^{s}\sum_{k=0}^{p}\sum_{n=1}^{\infty}n\int_0^{\alpha_1}f_{s-j,p-k,n}g_{j,k,n}\,\mathrm{d}\alpha \quad (20)$$

where $'$ denotes differentiation with respect to α. The advantage of expressions (19) and (20) over (15) is that to obtain the correction $Q_{s,p}$, we need only calculate terms up to order $(s, p-1)$. Expression (20) is especially convenient for use with MACSYMA. Needless to say, we use computer algebra to evaluate both the derivatives and the integrals in (20). As a result of our effort, we obtain a few analytical expressions for $Q_{s,p}$ as functions of α_1, i.e.

$$Q_{0,0} = \frac{2\pi}{\alpha_1}$$

$$Q_{0,1} = -\frac{2\pi}{a\alpha_1^2}$$

$$Q_{0,2} = \frac{2\pi}{a^2}\left(\frac{1}{\alpha_1^3}+\frac{\cosh\alpha_1}{2\alpha_1^2\sinh\alpha_1}\right).$$

Because of the considerable length of the analytical expressions for other $Q_{s,p}$, we do not reproduce them here (they can be obtained from us upon request). However, we do depict in Fig. 3 the corresponding numerical values of $Q_{s,p}$ as functions of the burial depth (d). We note that with an increase in d, there is a gradual increase of the values of $Q_{2,0}$ and $-Q_{3,0}$ whereas $-Q_{1,1}$ and $Q_{1,2}$ decrease very steeply. Having thus obtained the values of $Q_{s,p}$, we can calculate the heat flow for low Rayleigh numbers and high Biot numbers using the following formula:

$$Q = (Q_{0,0}+Bi^{-1}Q_{0,1}+Bi^{-2}Q_{0,2})$$
$$+Ra(Bi^{-1}Q_{1,1}+Bi^{-2}Q_{1,2})+Ra^2Q_{2,0}$$
$$+Ra^3Q_{3,0}+O(Bi^{-3}, RaBi^{-3}, Ra^2Bi^{-1}, Ra^4). \quad (21)$$

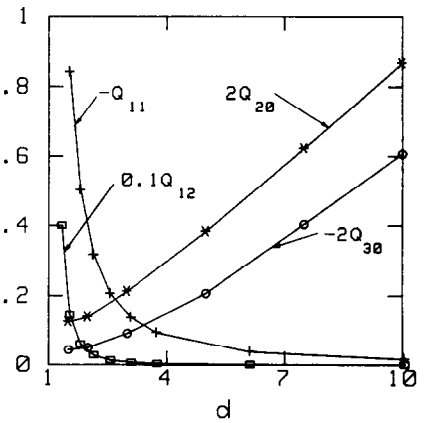

FIG. 3. The coefficients $Q_{1,1}, Q_{1,2}, Q_{2,0}$ and $Q_{3,0}$ depicted as functions of the burial depth (d).

In principle, additional terms could be calculated in (21) using the techniques outlined above; but as the order of approximation increases so do the demands on computer time and memory. We note in passing that even if many terms in the expansion were calculated, the expansion would not be valid for the full range of Biot and Rayleigh numbers since functions like $Q(Ra, Bi)$ typically have singularities lying in the complex Bi and Ra planes which limit their radii of convergence. With the limited number of terms we have, we are unable to find the radius of convergence of equation (21).

3.2. *Numerical solution—an expansion in Ra*

In this sub-section, we use equations (12) as our starting point. We noted earlier that these equations cannot be integrated analytically in a closed form. The same equations can, however, be integrated numerically. To this end, we use a second-order accurate finite-difference scheme. As a result of these calculations, we obtain the coefficients N_s in the Nusselt number expansion:

$$Nu = \sum_{s=0}^{\infty} N_s Ra^s \quad \text{where } N_0 \equiv 1. \tag{22}$$

All the calculations are carried out for two different grid sizes $(n \times n) = (45 \times 45)$ and (90×90). Although the equations solved are linear, it was necessary to use a relatively large number of grid points since the rate of convergence is adversely affected by the singularity at $(\alpha = \beta = 0)$, which corresponds to infinity in the physical plane.

The actual values of N_s are obtained using Richardson's extrapolation technique to zero grid size [12]. Briefly, in this method, N_s is considered to be a linear function of n^{-2}. The extrapolated value of N_s is obtained by taking the limit of N_s as $n \to \infty$. The procedure is described schematically in Fig. 4, where we depict values of N_2 and N_3 calculated at $\alpha = \alpha_1$

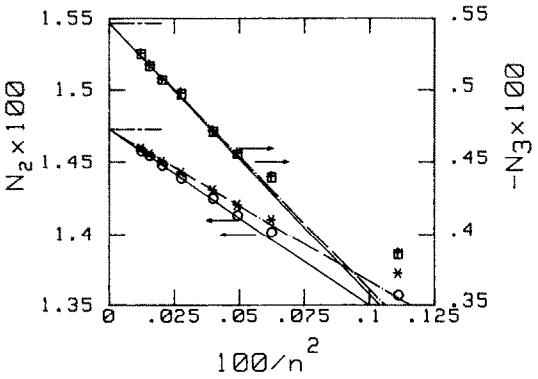

FIG. 4. Richardson's extrapolation of N_2 and N_3 to zero grid size. The solid line corresponds to the values calculated at the pipe's surface, while the dashed line represents the values next to the medium's surface. Burial depth (d) is 2 and Biot number (Bi) is ∞. Symbols correspond to the numerical data.

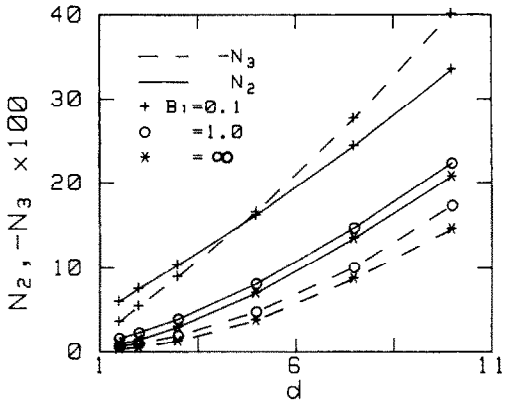

FIG. 5. The variation of N_2 and N_3 as a function of the burial depth (d) for different values of Biot number (Bi).

(solid lines) and $\alpha = \alpha_1/(n-1)$ (dashed lines) as functions of n^{-2} for a pipe buried at depth $d = 2$ beneath an isothermal surface ($Bi \to \infty$). In order to convince ourselves that N_s, indeed, behaves linearly with n^{-2}, we calculated N_s also for a number of intermediate values of n (i.e. $n = 30, 40, 50, 60$ and 70). The latter are depicted as symbols in Fig. 4. Clearly, a linear relationship exists between N_s and n^{-2} for $n > 30$.

We also compare the numerical results with the analytical ones (Section 3.1 and ref. [8]). The latter are depicted as horizontal dashed lines in Fig. 4, and they agree within 0.1% with the extrapolated values for N_s.

The results for N_2 and N_3 as a function of the burial depth d are depicted in Fig. 5 for $Bi = 0.1$, 1.0 and ∞. The coefficient $N_1 \equiv 0$ for $Bi = \infty$. For $0.1 \leqslant Bi \leqslant \infty$ and $d \geqslant 2$, N_1 is very small. Hence, in most practical cases, one may assume $N_1 \sim 0$ for all Biot numbers. This is in agreement with the analysis presented in Section 3.1. Both the absolute values of N_2 and N_3 increase as the burial depth increases and as the Biot number decreases. This indicates the growing relative importance of convection as d increases and/or Bi decreases.

Accurate estimation of the largest value of Ra (the radius of convergence denoted by Ra_c) for which the series (22) is still convergent is not feasible due to the small number of coefficients (N_s) available to us. The fact that N_2 and N_3 are of about the same order of magnitude suggests that $Ra_c \sim O(1)$. The range of utility of the series (22) based on comparison with the numerical solution of the non-linear equations (3) is given in Fig. 6 as a function of the Biot number. The radius of convergence increases with Biot number.

One can significantly increase the range of utility of the series (22) through the deployment of non-linear transformations. We use Shanks' transformation [14, 15] to obtain:

$$Nu = \frac{1 + ARa + BRa^2}{1 + ARa} \tag{23}$$

where $A = -N_3/N_2$ and $B = N_2$.

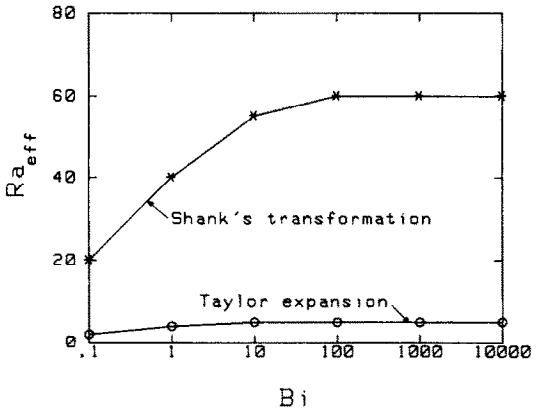

FIG. 6. The range of utility of Taylor expansions and Shanks' transformation for a hot pipe depicted as a function of the Biot number (Bi).

The values A and B can be calculated from Fig. 5 or by using the following correlation:

$$A = a_1 d^{a_2} \quad \text{and} \quad B = 10^{-2} d(b_1 d^{b_2} + b_3) \quad (24)$$

where

$$a_1 = 0.28 + (0.058/Bi) - (0.0029/Bi^2)$$

$$a_2 = 0.4 - (0.048/Bi) + (0.0042/Bi^2)$$

$$b_1 = 1.084 - (1.016/Bi) + (0.091/Bi^2)$$

$$b_2 = 0.393 + (0.593/Bi) - (0.053/Bi^2)$$

and

$$b_3 = 3.85 \tanh(0.45/Bi) - 0.71.$$

It turns out that, for the hot pipe ($Ra > 0$), Shanks' transformation increases the range of utility of expression (22) by at least an order of magnitude. The range of utility of Shanks' transformation is estimated by comparing results obtained from (23) with numerical solutions of the full non-linear equations. This range of utility is depicted in Fig. 6 as a function of the Biot number.

The results for the case of the cold pipe ($Ra < 0$) are not nearly as spectacular. Here, the range of utility of Shanks' transformation (23) is about the same as that of the series (22). This poor performance of Shanks' transformation is apparently a consequence of the fact that for $Ra < 0$, Shanks' transformation becomes singular at $Ra = -1/A$. This poor performance also can be explained on the basis of physical considerations. The perturbation expansion developed here assumes that the phenomena is conduction dominated. This is true in the case of the hot pipe. However, in the case of the cold pipe, convective effects may be more important than the conductive ones, and thus poor performance of the series solution may be expected.

Thus far, we have succeeded in obtaining a correlation for the Nusselt vs Rayleigh number [equation (23)] using perturbative analysis. The numerical solution of the non-linear equations serves as an important tool in the verification of the above correlation. In the next section, we briefly describe this numerical procedure.

4. SOLUTION OF THE NON-LINEAR PROBLEM

The governing differential equations (3), in conserving form, are converted into finite-difference equations. Central differences and Patankar's power-law technique are used to approximate the diffusive and convective terms, respectively [13]. The above numerical scheme is overall first-order accurate.

The grid system in the physical domain is shown in Fig. 1. Through the use of bicylindrical coordinates, the computational domain is transformed into a rectangle ($0 \leqslant \beta \leqslant \pi$, $0 \leqslant \alpha \leqslant \alpha_1$). A relatively large number of grid points are used here because the rate of convergence is adversely affected by the singularity at $\alpha = \beta = 0$ (the infinity in the physical plane). The number of grid points used ranges from 41×51 to 61×91 depending upon the value of the burial depth and the Darcy–Rayleigh number. For the higher effective Darcy–Rayleigh numbers and for negative Rayleigh numbers, one must use the large number of grid points.

We solve the finite-difference form of governing equations using successive over-relaxation [11]. For low effective Rayleigh numbers, the optimal over-relaxation parameter can be used [11]. As the effective Rayleigh number increases, however, we find it necessary to decrease the relaxation parameter in order to maintain numerical stability. The iterative procedure is terminated once the following convergence criterion was satisfied:

$$\max_{i,j} \left\{ \frac{\psi_{ij}^{n+1} - \psi_{ij}^{n}}{\psi_{ij}^{n+1}}; \frac{T_{ij}^{n+1} - T_{ij}^{n}}{T_{ij}^{n+1}} \right\} \leqslant \varepsilon.$$

ε was assigned the value 10^{-4} since the use of a more stringent condition did not make any significant difference in the solution. The number of iterations (typically between 200 and 1200) required to satisfy the above criterion varied with the effective Rayleigh number and the overrelaxation parameter. The very initial state consists of no motion and a conductive temperature distribution.

5. RESULTS AND DISCUSSION

In this section we describe the results of the numerical experiments (Section 4) as well as those of the perturbative analysis (Section 3). The first part of the section is devoted to a description of the temperature and flow fields while the second part deals with heat transfer. In the third part, we briefly discuss the range of validity of our results.

5.1. *Flow and temperature fields*

The temperature and flow fields associated with hot and cold buried pipes are depicted in Figs. 7–9. These are the results of the numerical simulation (Section 4).

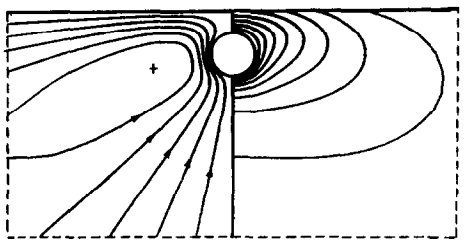

FIG. 7. Thermal convection around a hot buried pipe ($d = 2$, $Ra = 10$, $Bi = 1$). The uniformly spaced streamlines and isotherms are shown on the LHS and RHS of the figures, respectively.

Both the streamlines and isotherms are uniformly spaced.

Figures 7 and 8 describe, respectively, the cases of hot and cold pipes buried at a depth $d = 2$, with $Bi = 1$ and $|Ra| = 10$. In the case of the hot pipe (Fig. 7), the fluid adjacent to the pipe becomes hotter and thus tends to rise until it hits the top, cold surface. As the fluid travels along the cold, horizontal surface, it cools down and eventually descends to form a convective cell. On the other hand, in the case of the cold pipe (Fig. 8), the fluid adjacent to the pipe becomes colder and tends to sink. As the fluid descends, its temperature is equalized with the temperature of its surroundings until eventually it loses its negative buoyancy. Since fluid withdraws to the vicinity of the pipe due to pressure differences, once again we observe the development of a single convective cell. In the case of the hot pipe (Fig. 7), no plume structure develops at this low Rayleigh number ($Ra = 10$, $Ra_{\text{eff}} = 20$). In contrast, in the case of the cold pipe (Fig. 8), one observes a clear evolution of a plume structure. This difference is attributable to the fact that, in the case of the cold pipe, the convective motion is not constrained by a surface, while in the case of a hot pipe it is. Consequently, Ra_{eff} in Fig. 8 is considerably larger than the one in Fig. 7. As Ra_{eff} increases, a plume structure develops even in the case of the hot pipe as is evident from Fig. 9 ($Ra_{\text{eff}} = 100$).

In all our numerical experiments, we observed a flow structure consisting of two counter-rotating convective cells (Figs. 7–9). In the range of parameters, we considered, no two-dimensional bifurcations into multicellular convection were detected.

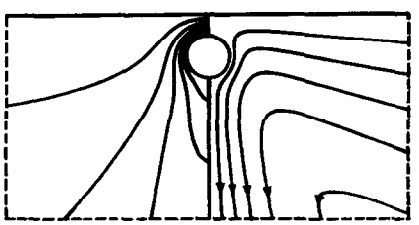

FIG. 8. Thermal convection around a cold buried pipe ($d = 2$, $Ra = -10$, $Bi = 1$). The uniformly spaced streamlines and isotherms are shown on the RHS and LHS of the figure, respectively.

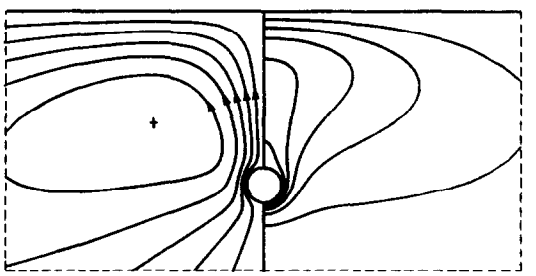

FIG. 9. Thermal convection around a hot buried pipe ($d = 10$, $Ra = 10$, $Bi = \infty$). Uniformly spaced streamlines and isotherms are shown on the LHS and RHS of the figure, respectively.

The temperature distribution along the top surface is depicted in Fig. 10. The upper and lower halves of the figure correspond, respectively, to hot ($Ra > 0$) and cold ($Ra < 0$) pipes. The effect of the Rayleigh number on the temperature distribution is shown on the RHS for $Bi = 1$, while the effect of the Biot number is depicted on the LHS for $|Ra| = 10$.

For $Bi \to \infty$, the temperature of the top surface remains uniform. As the Biot number decreases, the temperature deviates from uniformity and a Gaussian-like temperature distribution evolves. The temperature extreme occurs immediately above the pipe. For the hot and cold pipes, the temperature peak increases in magnitude as the Biot number decreases. As the Rayleigh number increases the temperature peak increases for the hot pipe while it decreases for the cold pipe. In the latter case, conduction causes a decline in the surface temperature while the convection tends to equalize the surface temperature. Thus, as the intensity of the convection increases (as the magnitude of Rayleigh number increases) the magnitude of the temperature extreme decreases.

5.2. *Heat transfer*

In this sub-section (Figs. 11–13), we compare the results obtained with the correlation [equation (23)] derived in Section 3 with those of the numerical

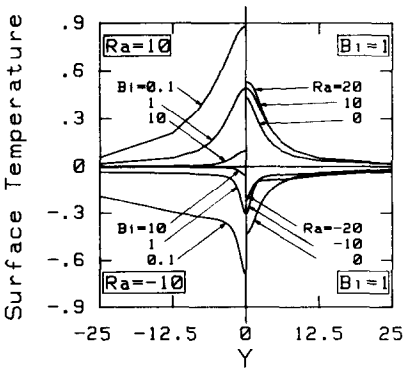

FIG. 10. Variation of the medium's surface temperature as a function of the horizontal distance (Y) from the pipe's axis for various values of Biot number (Bi) and Rayleigh number (Ra). The burial depth $d = 2$.

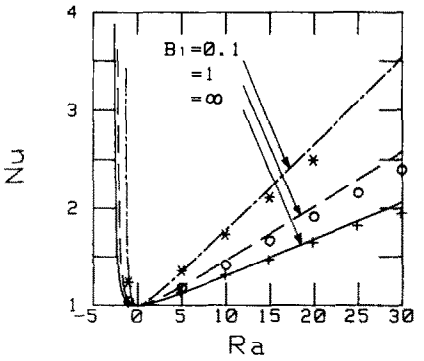

FIG. 11. The Nusselt number (Nu) is depicted as a function of the Rayleigh number (Ra) for various values of the Biot number (Bi) for burial depth $d = 2$. The curves correspond to the Shanks' transformation while the symbols represent the results of non-linear numerical simulation.

simulations (Section 4) as they pertain to the heat transfer problem.

The Nusselt number as a function of the Rayleigh number is depicted in Fig. 11 for hot and cold pipes buried at depth $d = 2$ for $Bi = 0.1$, 1 and ∞. The various curves correspond to the correlation [equation (23)] while the symbols represent the results of the numerical simulation (Section 4). Clearly, there is good agreement between the correlation and the numerical results. The range of utility of the correlation, depicted in Fig. 6, is determined as the largest Rayleigh number for which the difference between the correlation and the numerical simulation is smaller than 5%. The top and bottom curves in Fig. 6 indicate the range of utility of the correlation for the cases of the hot and cold pipes, respectively.

In Fig. 12, we depict the heat flow (Q) associated with hot and cold pipes buried beneath an isothermal surface ($Bi \to \infty$) as a function of the burial depth (d) for $Ra = -1$, 10, 20, 30 and 40. The solid lines in Fig. 12 represent the correlation (23) while the symbols denote the results of the numerical simulation. The dashed lines are provided for better readability and they connect the numerical data points. In the case of the hot pipe, the heat interaction (Q) decreases initially as the burial depth increases, reaches a minimum and then increases again, approaching asymptotically a value which corresponds to the heat losses associated with a pipe buried in an infinite medium (the horizontal broken lines on the RHS of Fig. 12). The asymptotic values for a pipe buried in an infinite, porous medium were obtained from Cheng's work [9]. Clearly, in the case of the hot pipe, there exists an optimal burial depth for which the heat losses are minimized. A similar optimum does not exist for the case of the cold pipe. Here, the heat losses (Q) decrease monotonically as the burial depth increases until they reach the asymptotic value associated with a pipe buried in an infinite medium.

A physical explanation for the existence of an optimal burial depth in the case of the hot pipe was given in ref. [9]. Briefly, the heat transfer process consists of both conduction and thermal convection. As the burial depth of the hot pipe increases, the conductive heat losses are reduced. At the same time, however, the effective Rayleigh number increases, which implies higher losses by convection. Consequently, there is an optimal value for which the total heat transfer is minimized. As we mentioned earlier, such an optimum does not exist in the case of the cold pipe. Although the conductive losses of the cold pipe are reduced as the burial depth increases, the convective losses remain about the same, a fact which excludes the existence of an optimum point.

In Fig. 13, we examine the effect of the Biot number on the heat transfer. We depict the heat losses (Q) as a

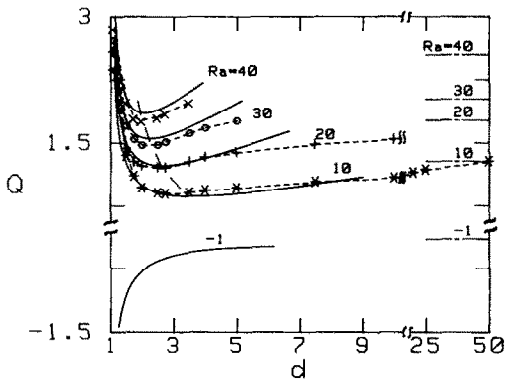

FIG. 12. The heat flow rate (Q) is depicted as a function of the burial depth (d) for $Bi = \infty$. Solid curves represent the correlation [equation (23)] while symbols represent the results of numerical experiments. The numerical data is connected with dashed lines. The asymptotic value for a pipe buried in an infinite, porous medium is denoted by the horizontal broken line on the RHS of the figure.

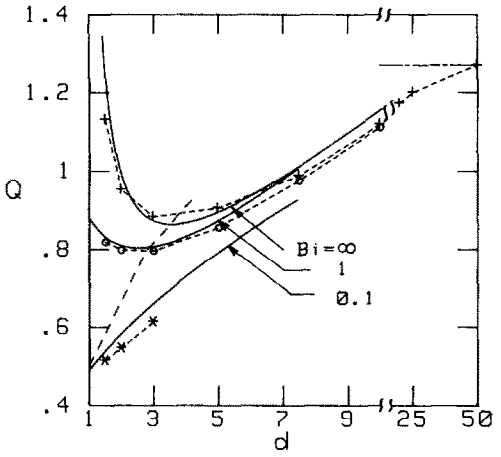

FIG. 13. The heat flow rate (Q) is depicted as a function of the burial depth (d) for $Ra = 10$ and for $Bi = 0.1$, 1 and ∞. Solid curves represent the correlation [equation (23)] while symbols represent the results of numerical experiments. The numerical data is connected with dashed lines. The asymptotic value for a pipe buried in an infinite medium is given by the horizontal broken line on the RHS of the figure.

function of the burial depth (d) for $Ra = 10$ and $Bi = 0.1$, 1 and ∞. The solid curves are the results of the correlation [equation (23)] while the various symbols represent the results of the numerical simulation (Section 4). The dashed line connects the numerical data points to facilitate a better appreciation of the trends. As the burial depth becomes large, all the curves approach asymptotically a common limit [9] which corresponds to a pipe buried in an infinite medium (the horizontal dashed line on the RHS of the figure). The magnitude of the optimal burial depth decreases as the Biot number decreases. For $Bi = 0.1$, we do not observe an optimal depth. Probably, this is because convection plays a larger and larger role in the heat transfer process as the Biot number decreases, while the conduction effects become less and less significant.

Finally, let us examine the contribution of thermal convection to heat losses from buried pipes. Consider, for example, a hot pipe, with a radius $\hat{r}_1 = 0.25$ m, buried in silica sand (grain size of about 2.54×10^{-4} m and permeability $\lambda \sim 6 \times 10^{-11}$ m^2) saturated with water. The temperature difference between the pipe and the earth's surface is $\hat{T}_1 - \hat{T}_2 = 60°C$. The corresponding Darcy–Rayleigh number is $Ra \sim 10$. For a pipe buried at depth 2 m ($\hat{d}/\hat{r}_1 = 8$), $Nu \sim 2.8$. Thus, the thermal convection represents two-thirds of the total heat losses.

5.3. *The range of validity of the results*

In this manuscript, we describe theoretical results which are based on the assumption that the flow is two-dimensional and steady. This, however, is the case only for a certain range of Rayleigh numbers. Experiments we are conducting in our laboratory indicate that there exists a critical Rayleigh number, beyond which the convective motion becomes three dimensional and oscillatory. For example, for burial depths of 7 and 14, the bifurcation into three-dimensional convection occurs at $Ra_{\text{eff}} \cong 90$ and 200, respectively. However, these values are somewhat larger than the range of utility of our correlation (Fig. 6).

Another matter of concern is the validity of the Darcy–Oberbeck–Boussinesq (DOB) equations for the range of Rayleigh numbers considered in this study. Darcy's law is considered to be valid for Reynolds numbers $Re < 10$, where $Re = \bar{u}_c d_p/\nu$. In the foregoing equation, d_p is a characteristic dimension of the porous media (i.e. pore or particle diameter) and $\bar{u}_c$ is the Darcian velocity. In our case, the maximum velocity is obtained next to the pipe and is $O[g\beta(\hat{T}_1 - \hat{T}_2)\lambda/\nu]$. Consequently, we conclude that the DOB equations are valid for

$$Ra < 10Pr\frac{r_1}{d_p}$$

where Pr is the Prandtl number. For example, in the case of water $Pr \sim 8$ and $r_1/d_p \sim 10^2$, the DOB equations are valid for $Ra_{\text{eff}} \sim O(10^3)$. This magnitude of the Rayleigh number is well above those considered in this study.

6. CONCLUSION

A theoretical solution has been provided for the flow and temperature fields around a pipe buried in a permeable medium, the surface of which is subject to Robin's boundary condition. Expressions for the streamfunction and temperature fields were provided using a double expansion in the Rayleigh number and the inverse of the Biot number. The analytical expressions were valid only for small Rayleigh ($Ra < 1$) and large Biot numbers. The restriction on the magnitude of the Biot number was removed by constructing numerically a perturbation expansion. This allowed us to derive a Taylor series for the Nusselt numbers in terms of the Rayleigh number. The range of validity of the above series was still restricted to small Rayleigh numbers. However, by using a non-linear transformation, we were able to considerably increase the range of utility of the series for hot pipes. Thus, we obtained a correlation for the Nusselt number as a function of burial depth, Rayleigh numbers and Biot numbers. The validity and range of utility of the correlation were established by comparison with numerical solutions of the non-linear equations.

Finally, we demonstrated that an optimal burial depth, which was originally observed in ref. [8] for the case of an isothermal medium surface, also exists for surfaces with convective boundary conditions. The magnitude of this optimal burial depth decreases as the Biot number decreases.

Acknowledgments—MACSYMA was developed by the Massachusetts Institute of Technology Mathlab group. The material presented here is based upon work supported, in part, by the National Science Foundation under Grant No. CBT 83-51658.

REFERENCES

1. E. R. G. Eckert and R. M. Drake, *Analysis of Heat and Mass Transfer*, pp. 92–102. McGraw-Hill, New York (1972).
2. N. N. Lebedev, I. P. Skalakaya and Y. S. Uflyand, *Worked Problems in Applied Mathematics*, pp. 212–214. Dover, New York (1979).
3. H. H. Bau and S. S. Sadhal, Heat losses from a fluid flowing in a buried pipe, *Int. J. Heat Mass Transfer* **25**, 1621–1629 (1982).
4. R. F. DiFelice and H. H. Bau, Conductive heat transfer between eccentric cylinders with boundary conditions of the third kind, *Trans. Am. Soc. mech. Engrs*, Series C, *J. Heat Transfer* **105**, 678–680 (1983).
5. V. E. Schrock, R. T. Fernandez and K. Kesavan, Heat transfer from cylinders embedded in a liquid filled porous medium, *Proc. Int. Heat Transfer Conference*, Paris, Vol VII, Ct. 3.6 (1970).
6. R. T. Fernandez and V. E. Schrock, Natural convection

from cylinders buried in a liquid-saturated porous medium, *Proc. Int. Heat Transfer Conference*, Munich, Vol. 2, pp. 335–340 (1982).
7. B. Farouk and H. Shayer, Natural convection around a heated cylinder buried in a saturated porous medium. In *Heat Transfer in Porous Media and Particulate Flows, Proc. 23rd National Heat Transfer Conference*, Denver, CO, ASME HTD Vol. 46 (1985).
8. H. H. Bau, Convective heat losses from a pipe buried in a semi-infinite porous medium, *Int. J. Heat Mass Transfer* **27**, 2047–2056 (1984).
9. Ping Cheng, Natural convection in a porous medium: External flows, presented at NATO Advanced Study Institute (July 16–27, 1984).
10. P. Moon and D. E. Spencer, *Field Theory Handbook*, pp. 64, 89. Springer, New York (1971).
11. P. J. Roache, *Computational Fluid Dynamics*. Hermosa, Albuquerque, NM (1976).
12. S. W. Churchill, P. Chao and H. Ozoe, Extrapolation of finite-difference calculations of laminar natural convection in enclosures to zero grid size, *Numer. Heat Transfer* **4**, 39–51 (1981).
13. S. V. Patankar, *Numerical Heat Transfer and Fluid Flow*. McGraw-Hill, New York (1982).
14. D. Shanks, Nonlinear transformations of divergent and slowly convergent sequences, *J. Math. Phys.* **34**, 1–42 (1955).
15. C. M. Bender and S. A. Orszag, *Advanced Mathematical Methods for Scientists and Engineers*, pp. 369–375. McGraw-Hill, New York (1978).

CONVECTION THERMIQUE ASSOCIEE AVEC DES CANAUX CHAUDS/FROIDS DANS UN MILIEU SEMI-INFINI, POREUX ET SATURE

Résumé—On présente des solutions analytiques et numériques pour la convection thermique permanente induite par des canaux chauds/froids dans un milieu poreux saturé, semi-infini, dont la surface est horizontale, imperméable et sujette à la condition limite de Robin. La surface du canal est imperméable et isotherme. La solution analytique concerne un double développement en termes de nombres de Rayleigh et de Biot inverse. L'ordinateur est utilisé pour les manipulations mathématiques les plus pénibles (MACSYMA). L'approche numérique implique à la fois la construction d'un développement régulier de perturbation en fonction du nombre de Rayleigh et la nature des équations complètes non linéaires. Les résultats des deux approches qui concernent la description des champs d'écoulement et de température ainsi que les valeurs du nombre de Nusselt, sont comparés et on trouve un accord satisfaisant.

THERMISCHE KONVEKTION AN HEISSEN/KALTEN ROHREN IN EINEM HALBUNENDLICHEN GESÄTTIGTEN PORÖSEN MEDIUM

Zusammenfassung—Es werden analytische und numerische Lösungen für die stationäre thermische Konvektion vorgestellt, welche durch heiße bzw. kalte Rohre in einem gesättigten halbunendlichen durchlässigen Medium induziert wird. Die Oberfläche des Mediums ist horizontal, undurchlässig und unterliegt den konvektiven Randbedingungen von Robin. Die Rohroberfläche ist undurchlässig und isotherm. Die analytische Lösung besteht aus einer doppelten Reihenentwicklung nach der Rayleigh- und der inversen Biot-Zahl. Die Computer-Algebra (MACSYMA) wurde zur Bewältigung der umfangreichen mathematischen Prozeduren verwendet. Das numerische Näherungsverfahren verwendet sowohl einen gewöhnlichen Störungsansatz mit einer Reihenentwicklung nach der Rayleigh-Zahl als auch die Lösung des vollständigen Satzes der nicht-linearen Erhaltungsgleichungen. Die Ergebnisse der Störungsanalysen und der numerischen Berechnungen, welche sowohl Beschreibungen des Strömungs- und Temperaturfeldes als auch Korrelationen für die Nusselt-Zahl enthalten, wurden verglichen und zeigen zufriedenstellende Übereinstimmung.

ТЕПЛОВАЯ КОНВЕКЦИЯ, ВЫЗВАННАЯ ГОРЯЧИМИ/ХОЛОДНЫМИ ТРУБАМИ, ПОГРУЖЕННЫМИ В ПОЛУБЕСКОНЕЧНУЮ НАСЫЩЕННУЮ ПОРИСТУЮ СРЕДУ

Аннотация—Получены аналитические и численные решения уравнений стационарной тепловой конвекции, обусловленной горячими/холодными трубами, погруженными в насыщенную полубесконечную проницаемую среду, ограниченную горизонтальной непроницаемой поверхностью, на которой выполняются граничные условия Робина. Поверхность трубы является непроницаемой и изотермической. Аналитическое решение основано на построении двойного разложения по параметрам Рэлея и Био. При выполнении более трудоемких математических расчетов использовалась вычислительная программа (MACSYMA). Численное решение включает как построение разложения регулярных возмущений по числу Рэлея, так и решение исходных нелинейных уравнений. Проведено сравнение результатов анализа возмущений и численных расчетов, описывающих поля течения и температуры, а также зависимостей для числа Нуссельта; найдено хорошее соответствие всех величин.